Journal of MATERIALS RESEARCH

Invited Paper
DOI: 10.1557/jmr.2019.76

INTRINSIC AND EXTRINSIC SIZE EFFECTS IN MATERIALS

FOCUS ISSUE

Grain size effects on dynamic fracture instability in polycrystalline graphene under tear loading

Yuxin Zhao[1], Yunfei Xu[2], Xiaoyi Liu[2], Jun Zhu[3,a)], Sheng-Nian Luo[4,b)]

[1]College of Physical Science and Technology, Sichuan University, Chengdu, Sichuan 610064, People's Republic of China; and The Peac Institute of Multiscale Sciences, Chengdu, Sichuan 610031, People's Republic of China
[2]The Peac Institute of Multiscale Sciences, Chengdu, Sichuan 610031, People's Republic of China
[3]College of Physical Science and Technology, Sichuan University, Chengdu, Sichuan 610064, People's Republic of China
[4]The Peac Institute of Multiscale Sciences, Chengdu, Sichuan 610031, People's Republic of China; and Key Laboratory of Advanced Technologies of Materials, Ministry of Education, Southwest Jiaotong University, Chengdu, Sichuan 610031, People's Republic of China
a)Address all correspondence to these authors. e-mail: zhujun01@163.com
b)e-mail: sluo@pims.ac.cn

Received: 30 November 2018; accepted: 13 February 2019

The stability of dynamic fracture is a fundamental and challenging problem in the field of materials science. The grain size effect on dynamic fracture instability in polycrystalline graphene under tear loading is explored via theoretical analysis and molecular dynamics simulations. The fracture stability phase diagram in terms of grain size and crack propagation velocity is obtained, and three regions of crack propagation are identified: stable, metastable, and unstable. For grain size above 2 nm, there exists a critical velocity beyond which fracture instability occurs, and this critical velocity depends linearly on grain size. Decreasing grain size leads to reduced characteristic time for correction of crack path deflection, which plays a dominant role in dynamic fracture instabilities. However, when grain size is below 2 nm, there does not exist a critical velocity for steady propagation of cracks due to discontinuous effects. Our results also provide a valuable insight into dynamic fracture of polycrystalline graphene as well as other 2D and quasi-2D materials.

Introduction

Our understanding of dynamic fracture mechanisms is facilitated by nanomechanics at the beginning of this century [1, 2, 3]. It has been demonstrated that the propagation of a Griffith crack can be predicted by the Yoffe's model in the case of harmonic and linear elastic materials [4, 5, 6] and by the Gao's model in the case of hyperelastic materials [7, 8, 9]. In recent years, the interface effects on dynamic fracture have been of considerable interest. In 2017, Rezaei et al. constructed a mechanical model to predict fracture and damage in micro-/nanocoating systems by using the cohesive zone element technique implemented at grain boundaries as well as in the interface between the coating and the substrate [10]. Daniel et al. found that the fracture toughness of ceramic nanostructured materials can be improved more than 150% by a dedicated grain boundary orientation design with respect to the direction of the expected crack path without the loss of hardness [11]. Through atomistic study, Tehranchi et al. studied the underlying mechanism of hydrogen embrittlement of grain boundaries in nickel [12]. In particular, grain boundaries are ubiquitous and influence the growth and propagation of cracks [13], since the interface energy plays a key role in fracture [14].

The complexities due to the three-dimensional (3D) nature of grains and cracks render it challenging to understand the mechanisms of crack propagation in materials with grain boundaries [15, 16, 17]. For simplicity, some fundamental mechanisms can be revealed via studying the crack propagation of 2D or quasi-3D materials [18, 19, 20]. In 2004, graphene, the first 2D material, was discovered [21]. Due to its fascinating properties such as extremely high electron mobility [22], high strength [23], high elasticity [24], quantum electronic transport [25], and electromechanical modulation [26], graphene has been of sustained interest. Through nanoindentation experiments, Lee et al. [23] measured the in-plane tensile properties of graphene: its Young's modulus is about 1.0 ± 0.1 TPa, and its strength is about 130 ± 10 GPa. From the atomic force microscope (AFM) experiments by Tanenbaum et al. [27], the spring constants of graphene are obtained as 1–5 N/m, the

https://doi.org/10.1557/jmr.2019.76 Published online by Cambridge University Press

© Materials Research Society 2019

equivalent Young's modulus of doubly clamped beams under tension is estimated as 0.5 TPa, and the in-plane Young's modulus of graphene is determined to be about 1.0 TPa. Since graphene is a 2D structure with a single layer of carbon atoms arranged in a hexagonal lattice, it is an ideal model material to investigate dynamic fracture in a 2D discrete atomistic system. On the one hand, this 2D nanostructure can reduce the variables in the theoretical mechanical model and simplify the problem. On the other hand, for molecular dynamics (MD) simulations, the in-plane dimensions can be taken to be adequately large (e.g., up to micrometers) to minimize the sample size effects on both the fracture modes and loading without significantly increasing the computational cost.

Considerable efforts have already been dedicated to crack evolution in graphene to investigate the fundamental mechanisms of dynamic fracture in 2D materials [28, 29, 30]. In general, cracks propagate along the zigzag direction in pristine graphene following the path of the minimal fracture surface energy [31, 32]. In 2005, Wei et al. found that the Griffith criterion remains valid for cracks down to 10 nm but overestimates the strength of shorter cracks [33]. In this situation, the local strength-based failure criterion is more suitable than energy-based Griffith criterion in describing crack propagation in graphene. Actually, the discontinuous effect in graphene is ubiquitous and highly affects the mechanical behavior such as transverse waves [34], buckling [35], and twisting [36]. Different from ordinary 3D materials, the fracture surface energy of graphene is due to in-plane breaking of carbon–carbon bonds [33, 37]. Hence, grain boundaries (a type of atomistic defects) may have a pronounced effect on fracture of graphene [38]. Although Ruoff et al. found that the tilt grain boundaries with large angles do not have significant impact on the fracture strength of graphene [39], the defects may lead to crack propagation [40]. The experiments conducted by Lopez-Polin et al. suggest defect control as an approach to avoid catastrophic failure in graphene [41]. In general, cracks in pristine graphene can propagate steadily at low speeds and create atomically flat mirror-like surfaces [42]. However, physical disturbances (e.g., temperature, defects, loading) can result in fracture instabilities with irregularly faceted surfaces [43]. In addition, there are three basic ways of applying a force to enable crack propagation: opening (mode I), sliding (mode II), and tearing (mode III). Mode I fracture of graphene is the most studied problem at present based on the Griffith criterion [15]. Dynamic fracture instabilities of polycrystalline graphene have rarely considered grain size effects, especially for tear loading, which is still one of the significant yet unresolved issues related to the fracture of graphene [44].

In this work, we conduct MD simulations and theoretical analysis to investigate the grain size effects on dynamic fracture instabilities of graphene monolayer under tear loading. For polycrystalline graphene with a specified grain size, as the nominal crack tip velocity increases to a critical value, dynamic fracture instability occurs, leading to deflection or branch of cracks. The critical velocity of instability is significantly affected by graphene grain size, and the underlying mechanisms of fracture instabilities are revealed. Our results would also provide a valuable insight into dynamic fracture of polycrystalline graphene as well as other 2D and quasi-2D materials.

Results and discussion

Dynamic fracture of polycrystalline graphene under tear loading

MD simulations are performed to explore dynamic fracture of polycrystalline graphene as well as pristine graphene. Three representative samples (Fig. 1) are selected to show different fracture behaviors under tear loading. For pristine graphene, dynamic fracture instability is difficult to occur under tear loading, consistent with a previous result [45]. In a pristine graphene sheet, crack propagates along the zigzag direction due to the minimal fracture surface energy (10 J/m^2) [46]. When the initial crack is not along the zigzag direction, although the crack surfaces are not strictly mirror-like, they are usually periodically bent along the zigzag direction after deflection corrections. Thus, the crack still approximately propagates along a straight line (here this line is the axle line of the graphene sheet). This is also consistent with a previous study [33]. According to macroscopic mechanical theory, the crack should propagate along the axle line of graphene sheet under tear loading. For polycrystalline graphene, crack may propagate along a straight line [Fig. 1(a)], deflect toward boundary due to instability [Fig. 1(b)], or branch [Fig. 1(c)], depending on grain size D and crack tip velocity v_t. In general, deflecting and branching of cracks are considered as the two main types of dynamic fracture instabilities [1]. However, since the MD simulation is performed at room temperature, there inevitably exists physical disturbance induced by thermal fluctuations. Crack propagation is a highly localized mechanical behavior of materials and insensitive to the far field. According to our MD simulations, at different dimensions (W, L) of graphene sheet (W = 50, 100, and 200 nm, and L = 200, 400, and 600 nm), the deflection of stable cracks is generally less than 10 nm, similar to literature results [33]. Thus, in the following discussion of a straight line, we allow a deviation of $\pm$10 nm along the y-axis from this line. As long as the crack path fluctuates within this range and eventually reaches the end of region V, the crack propagation is considered steady.

In Yoffe's and Gao's theories, crack tip velocity is considered to play a dominant role in dynamic fracture [1, 4, 5, 6]: for brittle materials, the Griffith cracks moving at low speeds create atomically flat mirror-like surfaces; at higher speeds, rougher,

https://doi.org/10.1557/jmr.2019.76 Published online by Cambridge University Press

© Materials Research Society 2019

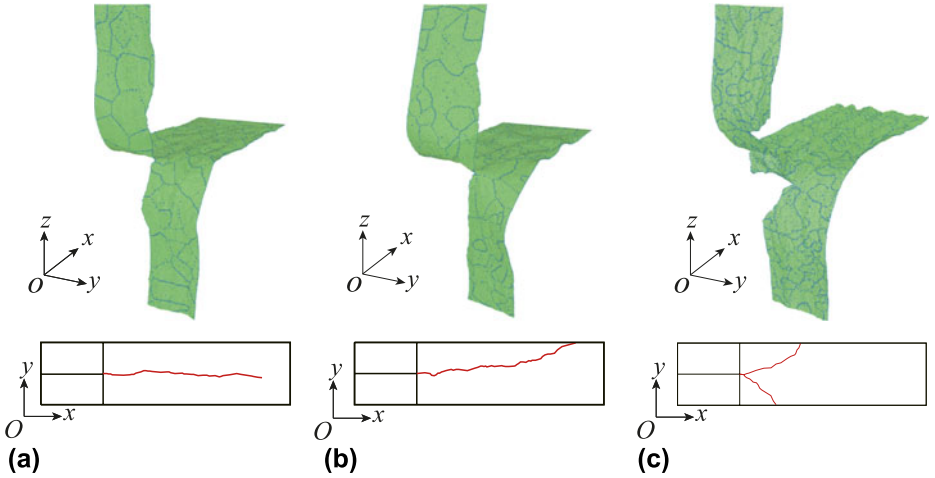


Figure 1: Atomic configurations of propagating cracks (top row) and crack tip trajectories (bottom row) in polycrystalline graphene with (a) $D = 11.3$ nm and $v_t = 1.7$ km/s (straight propagation), (b) $D = 9.0$ nm and $v_t = 1.1$ km/s (crack deflection), and (c) $D = 2.3$ nm and $v_t = 1.8$ km/s (crack branching).

less reflective (mist) and finally very rough, irregularly faceted (hackle) surfaces form. Although the in-plane strength of graphene is extremely high [23], its toughness is close to that of brittle materials [47]. Thus, crack can propagate along a straight line when v_t is below a critical velocity v_t^{crit}, while it deflects or branches when v_t is above v_t^{crit}. For a Griffith crack, v_t^{crit} is normally less than 73% of the Rayleigh wave speed. Similar phenomena occur for crack propagation in graphene under tear loading. For the same polycrystalline graphene sheet with $D = 11.3$ nm, when $v_t < 1.7$ km/s, cracks approximately propagate along straight lines in a narrow interval -5 nm $< y < 7.5$ nm (Fig. 2). When $v_t > 1.8$ km/s, the crack deflects rapidly to the boundary, which leads to a separation of one piece of graphene. This indicates that, under tear loading, there also exists a critical velocity v_t^{crit} beyond which crack instability occurs, in the forms of deflection or branching of cracks. Below v_t^{crit}, crack can propagate steadily, roughly along a straight line. Although there are some deflections along the y-axis, the cracks with $v_t < 1.8$ km/s eventually reach the end of region V, but not the boundaries along the y-axis. Thus, according to the definition above, the propagation of these cracks is considered steady.

To understand the atomistic mechanisms of crack stability or instability, crack propagation details for $D = 11.3$ nm at $v_t = 1.7$ km/s and $v_t = 1.8$ km/s are compared in Fig. 3. At $v_t = 1.7$ km/s, the crack surfaces are flat [Fig. 3(a)]. Although the potential energy of atoms at grain boundaries is higher than that of other atoms, the propagation of crack is not influenced by grain boundaries. In this case, the macroscopic force plays a dominant role in crack evolution. According to the analytical solution based on the symmetry theory [4], crack should propagate along the central axis of the graphene sheet (a straight line). However, due to thermal fluctuations at the nanoscale, it is impossible for the crack to propagate strictly

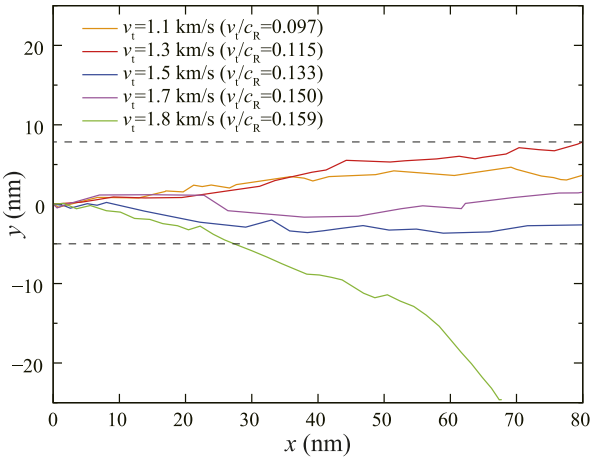


Figure 2: Crack propagation paths in the same polycrystalline graphene sheet with $D = 11.3$ nm at different v_t.

along a straight line, so small deviations from the expected straight are observed (Fig. 2). This is also consistent with a previous study on the Griffith crack propagation [43]. At $v_t = 1.8$ km/s, the crack surfaces become severely roughened [the red circles in Fig. 3(b)]. When the crack encounters a grain boundary parallel to the propagation direction, its tip deflects to one side of this grain boundary [$t = 32$ ps in Fig. 3(b)]. However, the crack tip cannot cross this parallel grain boundary again [$t = 38$ ps in Fig. 3(b)]. In this situation, the crack can only deflect to one side of the graphene sheet, and eventually the tear loading is balanced by dynamic fracture instability [$t = 60$ ps in Fig. 3(b)]. In other words, once v_t is above v_t^{crit}, the deflection of crack is rapidly amplified by grain boundaries, which are directly related to grain size D.

The response of polycrystalline graphene under tear loading gives rise to two issues: three types of crack propagation (straight, deflecting, and branching) are observed at different

https://doi.org/10.1557/jmr.2019.76 Published online by Cambridge University Press

© Materials Research Society 2019

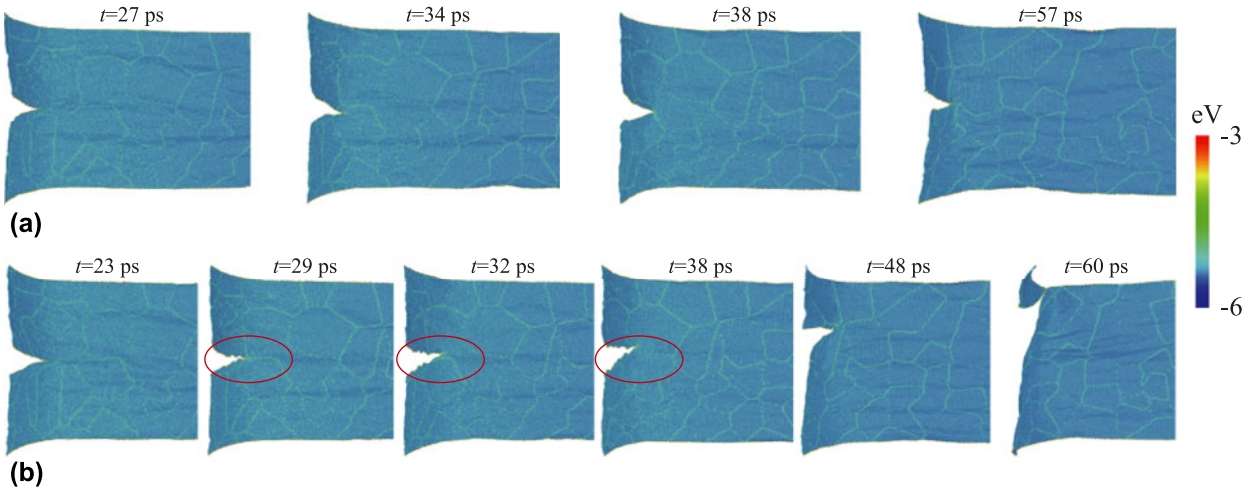


Figure 3: Crack propagation snapshots in polycrystalline graphene with $D = 11.3$ nm at (a) $v_t = 1.7$ km/s and (b) $v_t = 1.8$ km/s. Color coding refers to potential energy.

(v_t, D); for a specific grain size, the crack propagation becomes unstable as v_t increases to a critical value v_t^{crit}. Thus, it is necessary to perform MD simulations at different (v_t, D) to reveal the underlying mechanism of these two issues.

Grain-induced instability of dynamic fracture

The analysis presented in the previous section indicates that for a specified grain size D, there exists a critical value of v_t, i.e., v_t^{crit}, beyond which fracture instability occurs. Thus, the stability of a crack is affected by both grain size D and its propagation velocity v_t (which in turn depends on load σ). To explore the effects of these two factors, thousands of MD simulation runs are performed at different (v_t, D) values. As mentioned in section "Models and methods," multiple polycrystalline graphene configurations with the same grain size are constructed for simulations under the same conditions. However, even for a given grain size D, the configurations generated by phase field crystal (PFC) simulations are different in grain boundary distribution due to the randomness of grain seeds. Thus, for the configurations with the same D but different grain boundary characteristics, their critical velocities v_t^{crit} are different.

The stability phase diagram of $\Psi(D, v_t)$ is obtained in Fig. 4 (a). This diagram can be divided into three regions: stable, metastable, and unstable. In the stable region, the cracks approximately propagate along a straight line in a narrow y-range, -10 nm $< y <$ 10 nm. In the unstable region, the cracks deflect toward the boundaries or branch rapidly. In the metastable region, both metastable and stable cracks are observed at a same (v_t, D) pair. The stable and unstable regions are separated by this metastable region. The metastable region is related to random grain boundary characteristics, an unsolved and complex problem in fracture mechanics [15, 28]. The stability of crack is determined by grain size D, tip velocity v_t and grain boundary characteristics. However, it is challenging to incorporate grain boundary characteristics in mechanical models [48]. Thus, we use probability Ψ to consider the effects of grain boundary characteristics. For the polycrystalline graphene with a specified grain size D, there are upper $\left(v_t^{crit+}\right)$ and lower $\left(v_t^{crit-}\right)$ limits for critical tip velocity v_t due to the existence of a metastable region. When $v_t > v_t^{crit+}$ or $v_t < v_t^{crit-}$, the effects of grain boundary characteristics can be neglected. In the case of $v_t > v_t^{crit+}$, dynamic fracture instability occurs regardless of grain boundary characteristics. In the case of $v_t < v_t^{crit-}$, the crack can propagate steadily without deflection or branching, regardless of grain boundary characteristics. When $v_t^{crit-} < v_t < v_t^{crit+}$, the stability of a crack is specimen dependent due to grain boundary effects. Defining the critical velocity of crack instability in a strict sense, we take $v_t^{crit} = v_t^{crit+}$ in the following discussion, since it is still possible for cracks to propagate steadily when $v_t^{crit-} < v_t < v_t^{crit+}$. This is also consistent with the results in previous studies [1, 28, 49].

We plot the critical velocity $\left(v_t^{crit}\right)$ as a function of grain size D in Fig. 4(b). v_t^{crit} increases with increasing D, and $v_t^{crit}(D)$ can be approximately described with a linear relation. For $D <$ 2 nm (MD simulations with $v_t < 0.6$ km/s are performed), there does not exist a critical velocity for steady crack propagation in polycrystalline graphene. Actually, Gao et al. found that, when the grain size was overly small, crack path becomes completely unpredictable, even though theoretically, there are stress concentration areas [49]. In such cases, critical grain size dominates dynamic fracture of polycrystalline graphene. Our MD simulations [Fig. 4(b)] suggest a critical grain size of ~2.0 nm; this value is also close to the out-of-plane discontinuous effect scale of graphene [35]. In addition,

https://doi.org/10.1557/jmr.2019.76 Published online by Cambridge University Press

© Materials Research Society 2019

when characteristic scale is less than 2 nm, there will be a strong discontinuous effect in graphene [34]. Thus, this phenomenon is consistent with the discontinuous effects proposed by the previous studies [34, 35, 49].

Although potential energy of atoms at grain boundaries is higher than that of other atoms, surface (fracture) energy is not significantly affected [39]. When crack propagates steadily, transgranular and intergranular fractures exist simultaneously [Fig. 5(a)]. As discussed in section "Dynamic fracture of polycrystalline graphene under tear loading," crack always propagates along the zigzag direction due to the minimal surface energy. When grain size is sufficiently large [the inset in Fig. 5(a)], there exists a space for crack to propagate alternately in different zigzag directions under tear loading: a small deflection from the x-axis is corrected to the central axis within a horizontal length λ (along the x-axis). In this situation, macroscopic structural stress plays the dominant role. However, when the grain size is extremely small [Fig. 5(b)], before the crack tip starts to be corrected, it encounters a grain boundary, which delays the correction process with an additional deflection. Thus, the deflection of crack could not be corrected, and eventually dynamic instability occurs. Gao's models suggest that there exists a characteristic time scale Δt for dynamic fracture [7, 8, 9], and $\Delta t = \lambda/v_t$, where $\lambda < D$. As D decreases, the maximum λ_p allowed and critical velocity v_t^{crit} decrease. Thus, the critical velocity v_t^{crit} can be estimated as follows:

$$v_t^{crit} = \lambda_p/\Delta t \approx D/\Delta t \Rightarrow v_t^{crit} \propto D \quad . \tag{1}$$

This is consistent with the linear relationship between v_t^{crit} and D [Fig. 4(b)]. It should be noted that the effect of grain boundary characteristics is not considered in the discussion above, since we mainly focus on the cases of $v_t > v_t^{crit+}$. Grain boundary characteristics and grain size generally affect intergranular and transgranular fractures in polycrystalline graphene. However, as shown in Fig. 5(b), beyond the critical velocity, intergranular and transgranular fractures occur simultaneously. Thus, this linear relationship is valid for predicting the upper limit of critical velocity. The metastable region is highly influenced by grain boundary characteristics and still remains an unsolved subject in fracture mechanics.

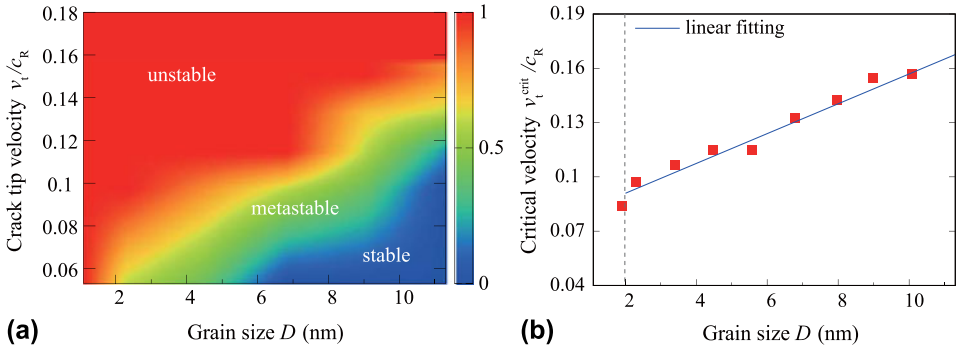


Figure 4: (a) $D - v_t$ diagram of crack stability parameter Ψ for polycrystalline graphene. $\Psi = 0$: stable, $\Psi = 1$: unstable, and $0 < \Psi < 1$: metastable. (b) $v_t^{crit} - D$ curve of polycrystalline graphene. Critical velocity v_t^{crit} increases with increasing grain size D.

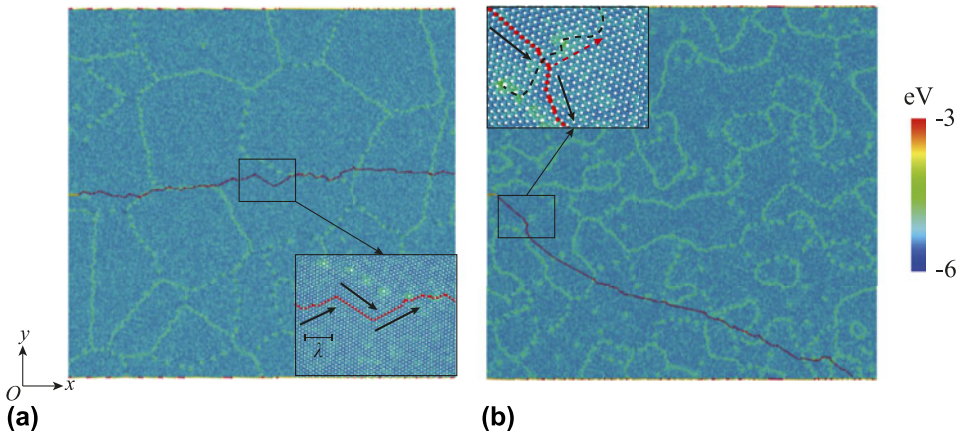


Figure 5: (a) Steady crack propagation for $D = 11.3$ nm. (b) Deflection of crack propagation for $D = 4.5$ nm. The atoms on crack surfaces are colored red. Insets: black line arrows, red dotted arrows, and black dotted lines represent crack propagation directions, corrected propagation directions, and grain boundaries, respectively.

https://doi.org/10.1557/jmr.2019.76 Published online by Cambridge University Press

© Materials Research Society 2019

Conclusion

Dynamic fracture instability in polycrystalline graphene is explored at different crack tip velocities and grain sizes (up to 11 nm). The crack instability phase diagram $v_t - D$ is obtained, consisting of stable, metastable, and unstable regions. For a given grain size ($D \geq 2$ nm), there exists a critical velocity v_t^{crit}, beyond which dynamic fracture instability occurs with roughened fracture surfaces. v_t^{crit} depends linearly on grain size: $v_t^{crit} \approx D/\tau$. Decreasing D leads to reduced characteristic time τ for deflection correction, which plays a dominant role in dynamic fracture instabilities. When $D < 2$ nm, there does not exist a critical velocity v_t^{crit} for steady propagation of cracks due to discontinuous effects.

Models and methods

Molecular dynamics simulation

Realistic polycrystalline graphene configurations are obtained from PFC simulations with a code developed by Hirvonen et al. [50]. The average grain size D is estimated as $\sqrt{4S/N\pi}$, where S is the total area of polycrystalline graphene and N is the number of grains. Grain boundary atoms have higher potential energy than other atoms [Fig. 6(a)]. Periodic boundary conditions are applied along the y-axis to ensure a zero pressure conditions with a vacuum space of 2 nm [Fig. 6(b)]. Fixed boundary conditions are applied along the x- and z-axes with a sufficiently large vacuum space (the dimensions of a simulation box are fixed along the x- and z-axes). A pair of uniaxial stresses with opposite directions but the same amplitude, $\pm\sigma$, is applied in regions I and II, respectively. The lengths of regions I and III along the z-axis are set at 12 nm. The atomic interactions between regions III and IV [Fig. 6(b)] are excluded to generate an initial crack, and cracks propagate in region V. The crack propagation is mainly characterized in region V, and the length of this region is over 100 nm to allow for sufficiently long evolution of cracks. The end of region V is fixed to avoid wrinkling during relaxing and tearing simulations. The width of polycrystalline graphene sheet W is set to 50 nm. Since there exist deflection and branching of cracks (see below), we define the nominal crack tip velocity, v_t, as the component of the real crack tip velocity along the x-axis. The nominal crack tip velocity v_t can be regulated by changing σ, which increases with increasing σ. Stable cracks propagate approximately along the x-axis, and v_t is close to the real crack tip velocity. For unstable cracks, v_t is still close to the initial real crack tip velocity.

The MD simulations are performed with an open source code LAMMPS [51]. We use the Stillinger–Weber (SW) potential recently developed by Hossain et al. for graphene [52], which can describe the elasticity and fracture of graphene as accurately as the adaptive intermolecular reactive empirical bond order (AIREBO) potential [53]. Thus, here we choose this SW potential to describe the atomic interactions between carbon atoms. The time step of all MD simulations is set to 1 fs. Visualization is achieved with OVITO [54]. Before tear simulations, the initial configurations are relaxed with the isothermal–isobaric (NPT) ensemble under periodic boundary conditions in the xy-plane for 100 ps at 300 K, and the pressure is set to 0 to ensure no initial stress in the graphene sheet. The tear simulations are performed with the microcanonical (NVE) ensemble, and the periodic boundary conditions are still applied along the y-axis to ensure a zero pressure (a vacuum space of 2 nm is added). Therefore, there is only one crack in the graphene sheet (in the middle). For statistics, we construct multiple polycrystalline configurations (over 5) for a given grain size. Each configuration contains 100–10,000 grains in a 50×200 nm^2 graphene sheet, corresponding to grain size D ranging from 1.1 to 11.3 nm (D = 1.1, 2.2, 4.5, 6.8, 9.0, or 11.3 nm). The crack tip velocity v_t ranges from 0.6 to 1.8 km/s (0.6, 1.1, 1.3, 1.5, 1.7, 1.75, 1.8 km/s). The theoretical Rayleigh wave speed of pristine graphene c_R is about 11.3 km/s regardless the out-of-plane deformation, and the maximum crack speed of graphene can reach about 0.71 c_R (~8.0 km/s) [55]. According to our MD simulations, when v_t is over 1.8 km/s, mode I crack may be induced. Thus, the maximum v_t is set to 1.8 km/s. All the data presented in the discussion below are statistically averaged unless otherwise stated.

Statistical analysis

Crack tip field plays a dominant role in crack propagation [56] and strongly depends on microstructure (e.g., the distribution of grain boundaries). However, there is not a method to effectively incorporate complex microstructure into mechanical parameters yet. Fracture stability of graphene sheet under tear loading can be considered as a generalized function:

$$\Psi = \Psi(\boldsymbol{G}, v_t;\ C) \quad , \tag{2}$$

where C is known physical constants (e.g., atomic interaction between carbon atoms and temperature) and $\boldsymbol{G}$ represents microstructure of polycrystalline graphene. In this work, $\boldsymbol{G}$ is a set consisting of n elements:

$$\boldsymbol{G} = \{G_1, G_2, G_3, \cdots, G_n\} \quad , \tag{3}$$

where G_i (i = 1, 2, 3,. . ., n) represents the ith "microstructure." Thus,

$$\boldsymbol{\Psi} = \{\Psi_1, \Psi_2, \Psi_3, \ldots, \Psi_n\} \quad . \tag{4}$$

However, according to our MD results and previous studies [47], Ψ_i is probably different from that of Ψ_j at $i \neq j$. Although G for thousands (or more) of microstructures can be obtained

https://doi.org/10.1557/jmr.2019.76 Published online by Cambridge University Press

© Materials Research Society 2019

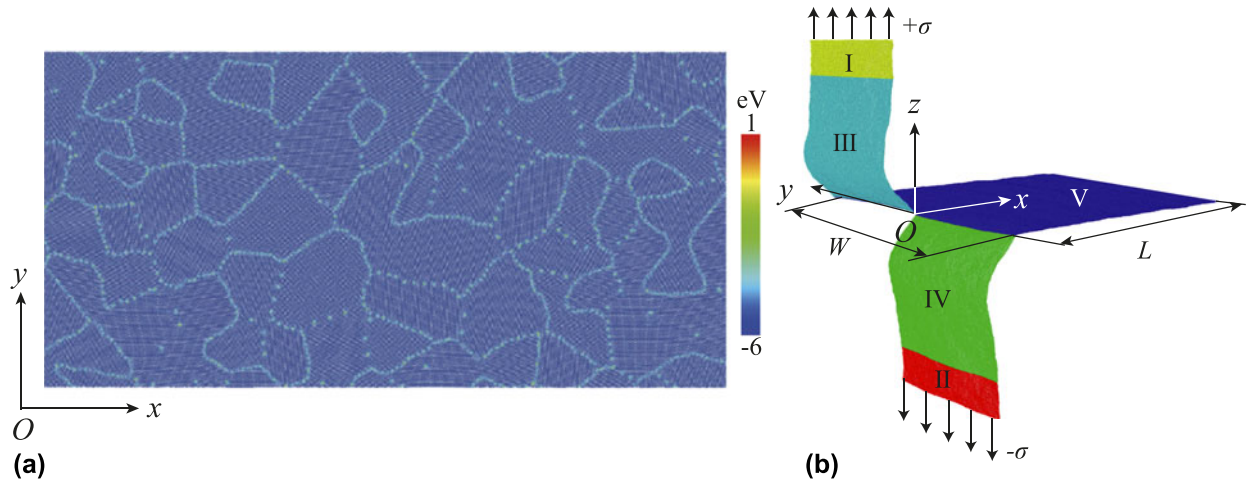


Figure 6: (a) Partial configuration of polycrystalline graphene generated by PFC simulations. Color coding referred represents potential energy. (b) Schematic of tearing loading of polycrystalline graphene. A pair of stress of opposite directions but the same amplitude, $\pm\sigma$, is applied in regions I and II, respectively. The atomic interactions between regions III and IV are excluded. Crack propagation is mainly characterized in region V.

regardless of the principle, there does not exist a universal mechanism or an effective way to incorporate all of them yet. Considering these issues above, we use probability to characterize fracture stability for an ensemble of specific microstructures, instead of an explicit quantitative function which is still nonexistent.

In this work, given multiple MD runs, we define the crack stability parameter, $\Psi \equiv N/M$, as the probability of crack instability at each ($\boldsymbol{G}$, v_t; C), where N and M are the numbers of unstable cracks and total cracks, respectively. The stability, metastability, or instability of a crack is defined as follows:

$$\Psi = \Psi(\boldsymbol{G},\ v_t;\ C) = \begin{cases} 0, & \text{stable} \\ 0-1, & \text{metastable} \\ 1, & \text{unstable} \end{cases} . \qquad (5)$$

The resultant Ψ is a set due to the effects of $\boldsymbol{G}$. For different samples, grain boundary characteristics are different at an identical D, but the corresponding grain boundary densities are approximately the same [57] (also see Table I). In experiments using the CVD method to fabricate polycrystalline graphene, the only controllable parameter is the areal density of grains, which is also referred to as the average grain size D. Therefore, $\boldsymbol{G}$ of polycrystalline graphene sheets with an identical D is still a set:

$$\boldsymbol{G}|_D\{G_1, G_2, G_3, \cdots, G_n\} \quad . \qquad (6)$$

Since it is still unrealistic to formulate an explicit function for $\boldsymbol{G}$ in terms of G_i, and D is a statistical representative of a microstructure, we choose D as the single material parameter to obtain Ψ statistically:

TABLE I: The grain boundary density and the atomic percent of dislocations at different D.

D (nm)	Grain boundary density (nm^{-1})	Atomic percent of dislocations
1.1	1.55 ± 0.01	10.48% ± 0.07%
2.2	1.46 ± 0.01	9.82% ± 0.07%
4.5	1.03 ± 0.01	6.90% ± 0.06%
6.8	0.74 ± 0.02	4.98% ± 0.15%
9.0	0.58 ± 0.01	3.90% ± 0.06%
11.3	0.49 ± 0.01	3.30% ± 0.08%

$$\Psi = \Psi(v_t, D) = \begin{cases} 0, & \text{stable} \\ 0-1, & \text{metastable} \\ 1, & \text{unstable} \end{cases} . \qquad (7)$$

Acknowledgments

This work was partially supported by the National Key R&D Program of China (Grant No. 2017YFB0702002), the Scientific Challenge Project of China (No. TZ2018001), and the National Natural Science Foundation of China (No. 11627901). The numerical calculations were performed at the Supercomputing Center of the Peac Institute of Multiscale Sciences.

References

1. **M.J. Buehler and H. Gao**: Dynamical fracture instabilities due to local hyperelasticity at crack tips. *Nature* **439**, 307 (2006).
2. **J. Swadener, M. Baskes, and M. Nastasi**: Molecular dynamics simulation of brittle fracture in silicon. *Phys. Rev. Lett.* **89**, 085503 (2002).
3. **T. Belytschko, S. Xiao, G. Schatz, and R. Ruoff**: Atomistic simulations of nanotube fracture. *Phys. Rev. B* **65**, 235430 (2002).

https://doi.org/10.1557/jmr.2019.76 Published online by Cambridge University Press

© Materials Research Society 2019

4. **L.B. Freund**: *Dynamic Fracture Mechanics* (Cambridge university Press, Cambridge, U.K., 1998).
5. **K.B. Broberg**: *Cracks and Fracture* (Elsevier, San Diego, California, 1999).
6. **E.H. Yoffe**: The moving Griffith crack. *Philos. Mag.* **42**, 739–750 (1951).
7. **H. Gao**: Surface roughening and branching instabilities in dynamic fracture. *J. Mech. Phys. Solids* **41**, 457–486 (1993).
8. **H. Gao**: A theory of local limiting speed in dynamic fracture. *J. Mech. Phys. Solids* **44**, 1453–1474 (1996).
9. **H. Gao**: Elastic waves in a hyperelastic solid near its plane-strain equibiaxial cohesive limit. *Philos. Mag. Lett.* **76**, 307–314 (1997).
10. **S. Rezaei, S. Wulfinghoff, and S. Reese**: Prediction of fracture and damage in micro/nano coating systems using cohesive zone elements. *Int. J. Solids Struct.* **121**, 62–74 (2017).
11. **R. Daniel, M. Meindlhumer, W. Baumegger, J. Zalesak, B. Sartory, M. Burghammer, C. Mitterer, and J. Keckes**: Grain boundary design of thin films: Using tilted brittle interfaces for multiple crack deflection toughening. *Acta Mater.* **122**, 130–137 (2017).
12. **A. Tehranchi and W. Curtin**: Atomistic study of hydrogen embrittlement of grain boundaries in nickel: I. Fracture. *J. Mech. Phys. Solids* **101**, 150–165 (2017).
13. **K. Leitner, D. Scheiber, S. Jakob, S. Primig, H. Clemens, E. Povoden-Karadeniz, and L. Romaner**: How grain boundary chemistry controls the fracture mode of molybdenum. *Mater. Des.* **142**, 36–43 (2018).
14. **D. Hull and D. Rimmer**: The growth of grain-boundary voids under stress. *Philos. Mag.* **4**, 673–687 (1959).
15. **T.L. Anderson**: *Fracture Mechanics: Fundamentals and Applications* (CRC Press, Boca Raton, 2017).
16. **D. Holland and M. Marder**: Ideal brittle fracture of silicon studied with molecular dynamics. *Phys. Rev. Lett.* **80**, 746 (1998).
17. **B.L. Holian and R. Ravelo**: Fracture simulations using large-scale molecular dynamics. *Phys. Rev. B* **51**, 11275 (1995).
18. **T. Bittencourt, P. Wawrzynek, A. Ingraffea, and J. Sousa**: Quasi-automatic simulation of crack propagation for 2D LEFM problems. *Eng. Fract. Mech.* **55**, 321–334 (1996).
19. **H. Rafii-Tabar, L. Hua, and M. Cross**: A multi-scale atomistic-continuum modelling of crack propagation in a two-dimensional macroscopic plate. *J. Phys.: Condens. Matter* **10**, 2375 (1998).
20. **R. Mas-Balleste, C. Gomez-Navarro, J. Gomez-Herrero, and F. Zamora**: 2D materials: To graphene and beyond. *Nanoscale* **3**, 20–30 (2011).
21. **K.S. Novoselov, A.K. Geim, S.V. Morozov, D. Jiang, Y. Zhang, S.V. Dubonos, I.V. Grigorieva, and A.A. Firsov**: Electric field effect in atomically thin carbon films. *Science* **306**, 666–669 (2004).
22. **K.I. Bolotin, K. Sikes, Z. Jiang, M. Klima, G. Fudenberg, J. Hone, P. Kim, and H. Stormer**: Ultrahigh electron mobility in suspended graphene. *Solid State Commun.* **146**, 351–355 (2008).
23. **C. Lee, X. Wei, J.W. Kysar, and J. Hone**: Measurement of the elastic properties and intrinsic strength of monolayer graphene. *Science* **321**, 385–388 (2008).
24. **K.S. Kim, Y. Zhao, H. Jang, S.Y. Lee, J.M. Kim, K.S. Kim, J-H. Ahn, P. Kim, J-Y. Choi, and B.H. Hong**: Large-scale pattern growth of graphene films for stretchable transparent electrodes. *Nature* **457**, 706 (2009).
25. **B. Özyilmaz, P. Jarillo-Herrero, D. Efetov, D.A. Abanin, L.S. Levitov, and P. Kim**: Electronic transport and quantum hall effect in bipolar graphene p-n-p junctions. *Phys. Rev. Lett.* **99**, 166804 (2007).
26. **J.S. Bunch, A.M. Van Der Zande, S.S. Verbridge, I.W. Frank, D.M. Tanenbaum, J.M. Parpia, H.G. Craighead, and P.L. McEuen**: Electromechanical resonators from graphene sheets. *Science* **315**, 490–493 (2007).
27. **I. Frank, D.M. Tanenbaum, A.M. van der Zande, and P.L. McEuen**: Mechanical properties of suspended graphene sheets. *J. Vac. Sci. Technol., B: Microelectron. Nanometer Struct.–Process., Meas., Phenom.* **25**, 2558–2561 (2007).
28. **T. Zhang, X. Li, and H. Gao**: Fracture of graphene: A review. *Int. J. Fract.* **196**, 1–31 (2015).
29. **D. Akinwande, C.J. Brennan, J. Scott Bunch, P. Egberts, J.R. Felts, H. Gao, R. Huang, J-S. Kim, T. Li, Y. Li, K.M. Liechti, N. Lu, H.S. Park, E.J. Reed, P. Wang, B.I. Yakobson, T. Zhang, Y-W. Zhang, Y. Zhou, and Y. Zhu**: A review on mechanics and mechanical properties of 2D materials—Graphene and beyond. *Extreme Mech. Lett.* **13**, 42–77 (2017).
30. **A. Gupta, T. Sakthivel, and S. Seal**: Recent development in 2d materials beyond graphene. *Prog. Mater. Sci.* **73**, 44–126 (2015).
31. **M-Q. Le and R.C. Batra**: Single-edge crack growth in graphene sheets under tension. *Comput. Mater. Sci.* **69**, 381–388 (2013).
32. **E. Orowan**: Fracture and strength of solids. *Rep. Prog. Phys.* **12**, 185 (1949).
33. **H. Yin, H.J. Qi, F. Fan, T. Zhu, B. Wang, and Y. Wei**: Griffith criterion for brittle fracture in graphene. *Nano Lett.* **15**, 1918–1924 (2015).
34. **X. Liu, F. Wang, and H. Wu**: Anisotropic propagation and upper frequency limitation of terahertz waves in graphene. *Appl. Phys. Lett.* **103**, 071904 (2013).
35. **X. Liu, F. Wang, and H. Wu**: Anisotropic growth of buckling-driven wrinkles in graphene monolayer. *Nanotechnology* **26**, 065701 (2015a).
36. **X. Liu, F. Wang, and H. Wu**: Anomalous twisting strength of tilt grain boundaries in armchair graphene nanoribbons. *Phys. Chem. Chem. Phys.* **17**, 31911–31916 (2015b).
37. **A.K. Geim**: Graphene: Status and prospects. *Science* **324**, 1530–1534 (2009).
38. **G-H. Lee, R.C. Cooper, S.J. An, S. Lee, A. Van Der Zande, N. Petrone, A.G. Hammerberg, C. Lee, B. Crawford, W. Oliver, J.W. Kysar, and J. Hone**: High-strength chemical-vapor–deposited graphene and grain boundaries. *Science* **340**, 1073–1076 (2013).

https://doi.org/10.1557/jmr.2019.76 Published online by Cambridge University Press

© Materials Research Society 2019

39. **R. Grantab, V.B. Shenoy, and R.S. Ruoff**: Anomalous strength characteristics of tilt grain boundaries in graphene. *Science* **330**, 946–948 (2010).
40. **M. Wang, C. Yan, L. Ma, N. Hu, and M. Chen**: Effect of defects on fracture strength of graphene sheets. *Comput. Mater. Sci.* **54**, 236–239 (2012).
41. **G. López-Polín, J. Gómez-Herrero, and C. Gómez-Navarro**: Confining crack propagation in defective graphene. *Nano Lett.* **15**, 2050–2054 (2015).
42. **M-Q. Le and R.C. Batra**: Crack propagation in pre-strained single layer graphene sheets. *Comput. Mater. Sci.* **84**, 238–243 (2014).
43. **P.R. Budarapu, B. Javvaji, V. Sutrakar, D. Roy Mahapatra, G. Zi, and T. Rabczuk**: Crack propagation in graphene. *J. Appl. Phys.* **118**, 064307 (2015).
44. **D. Sen, K.S. Novoselov, P.M. Reis, and M.J. Buehler**: Tearing graphene sheets from adhesive substrates produces tapered nanoribbons. *Small* **6**, 1108–1116 (2010).
45. **M.J. Moura and M. Marder**: Tearing of free-standing graphene. *Phys. Rev. E* **88**, 032405 (2013).
46. **R. Khare, S.L. Mielke, J.T. Paci, S. Zhang, R. Ballarini, G.C. Schatz, and T. Belytschko**: Coupled quantum mechanical/molecular mechanical modeling of the fracture of defective carbon nanotubes and graphene sheets. *Phys. Rev. B* **75**, 075412 (2007).
47. **P. Zhang, L. Ma, F. Fan, Z. Zeng, C. Peng, P.E. Loya, Z. Liu, Y. Gong, J. Zhang, X. Zhang, P.M. Ajayan, T. Zhu, and J. Lou**: Fracture toughness of graphene. *Nat. Commun.* **5**, 3782 (2014).
48. **L. Priester**: *Grain Boundaries: From Theory to Engineering*, Vol. **172** (Springer Science & Business Media, Dordrecht, 2012).
49. **T. Zhang, X. Li, S. Kadkhodaei, and H. Gao**: Flaw insensitive fracture in nanocrystalline graphene. *Nano Lett.* **12**, 4605–4610 (2012).
50. **P. Hirvonen, M.M. Ervasti, Z. Fan, M. Jalalvand, M. Seymour, S.M.V. Allaei, N. Provatas, A. Harju, K.R. Elder, and T. Ala-Nissila**: Multiscale modeling of polycrystalline graphene: A comparison of structure and defect energies of realistic samples from phase field crystal models. *Phys. Rev. B* **94**, 035414 (2016).
51. **S. Plimpton**: Fast parallel algorithms for short-range molecular dynamics. *J. Comput. Phys.* **117**, 1–19 (1995).
52. **M. Hossain, T. Hao, and B. Silverman**: Stillinger–weber potential for elastic and fracture properties in graphene and carbon nanotubes. *J. Phys.: Condens. Matter* **30**, 055901 (2018a).
53. **M.Z. Hossain, T. Ahmed, B. Silverman, M.S. Khawaja, J. Calderon, A. Rutten, and S. Tse**: Anisotropic toughness and strength in graphene and its atomistic origin. *J. Mech. Phys. Solids* **110**, 118–136 (2018b).
54. **A. Stukowski**: Visualization and analysis of atomistic simulation data with ovito–the open visualization tool. *Modell. Simul. Mater. Sci. Eng.* **18**, 015012 (2009).
55. **S. Xiao and T. Belytschko**: A bridging domain method for coupling continua with molecular dynamics. *Comput. Methods Appl. Mech. Eng.* **193**, 1645–1669 (2004).
56. **S.S. Terdalkar, S. Huang, H. Yuan, J.J. Rencis, T. Zhu, and S. Zhang**: Nanoscale fracture in graphene. *Chem. Phys. Lett.* **494**, 218–222 (2010).
57. **K.A. Brakke**: *Statistics of Random Plane Voronoi Tessellations* (Department of Mathematical Sciences, Susquehanna University, Pennsylvania, 1987). (Manuscript 1987a).

https://doi.org/10.1557/jmr.2019.76 Published online by Cambridge University Press

© Materials Research Society 2019